PHYSICAL REVIEW B **95**, 020405(R) (2017)

Electromagnon resonance in a collinear spin state of the polar antiferromagnet $Fe_2Mo_3O_8$

T. Kurumaji,[1] Y. Takahashi,[1,2,3] J. Fujioka,[2] R. Masuda,[2] H. Shishikura,[2] S. Ishiwata,[2,3] and Y. Tokura[1,2]
[1]*RIKEN Center for Emergent Matter Science (CEMS), Wako 351-0198, Japan*
[2]*Department of Applied Physics and Quantum Phase Electronics Center (QPEC), University of Tokyo, Tokyo 11-8656, Japan*
[3]*PRESTO, Japan Science and Technology Agency, Chiyoda, Tokyo 102-8666, Japan*
(Received 21 September 2016; published 5 January 2017)

Magnetic excitations are investigated for a hexagonal polar magnet $Fe_2Mo_3O_8$ by terahertz spectroscopy. We observed magnon modes including an electric-field active magnon, electromagnon, in the collinear antiferromagnetic phase with spins parallel to the c axis. We unravel the nature of these excitations by investigating the correlation between the evolution of the mode profile and the magnetic transition from antiferromagnetic to ferrimagnetic order induced by a magnetic field or Zn doping. We propose that the observed electromagnon mode involves the electric polarization oscillating within the c plane induced by the collective precession of the spins through the same mechanism as producing the linear magnetoelectric effect.

DOI: 10.1103/PhysRevB.95.020405

Cross correlation between magnetism and electricity, i.e., the magnetoelectric (ME) effect, is a key in designing electric-field-controllable spin devices [1,2]. Among various ME materials [3], multiferroics, which exhibit simultaneous magnetic and ferroelectric orders, have attracted tremendous interest because of recent discoveries of a strong ME response upon magnetic phase transition as in $TbMnO_3$ [4] as well as of room-temperature multiferroics, such as $BiFeO_3$ [5] and hexaferrite [6]. Entanglement between magnetism and electricity can be extended to elementary excitations, which was theoretically discussed since the 1970s [7]. In fact, the electric dipole-active magnon, termed the electromagnon, was observed as an infrared absorption in the terahertz region [8]. Such excitations have been identified in various multiferroic materials [9] and promise new terahertz functionalities of multiferroics including optical control of magnetism and nonreciprocal directional dichroism [10,11].

According to Khomskii [12], multiferroics can be classified into two types; in type-I multiferroics, the ferroelectricity and the magnetism has distinct origins, whereas the magnetic order itself is the driving force of ferroelectricity in type-II multiferroics. The former group includes $BiFeO_3$ and hexagonal $YMnO_3$ [5,13], which show relatively large spontaneous polarizations and high ferroelectric/magnetic transition temperatures, whereas the magnetism only modestly influences the polarization and/or dielectric constant. The latter group including orthorhombic (perovskite-type) RMnO$_3$ (R represents rare earth) [4,14], $Ni_3V_2O_8$ [15], and $MnWO_4$ [16] hosts strong ME coupling while tending to show relatively lower transition temperatures partly because of the frustration in spin interactions.

Early works on type-II multiferroics including RMnO$_3$ [8], hexaferrites [17], $TbMn_2O_5$ [18,19], and CuO [20] have clarified that incommensurate spiral magnetic orders generally exhibit the electromagnon resonances. Therein, a part of the electromagnons is driven by the exchange striction mechanism described by the inner product of spins, i.e., $\boldsymbol{S}_i \cdot \boldsymbol{S}_j$ [21], whereas the inverse Dzyaloshinskii-Moriya (DM) mechanism expressed by $\boldsymbol{S}_i \times \boldsymbol{S}_j$ also contributes to the electromagnon resonance with both electric and magnetic dipole activities [11]. Some magnetic materials host electromagnons even in a collinear magnetic phase or nonmagnetic paraelectric phase, which are in the vicinity of the type-II multiferroic phases, such as the helimagnetic ferroelectric phase or the collinear ferroelectric phase, respectively. Examples for the former material are orthorhombic RMnO$_3$ ($R = Y$ and Lu) [22] and $CuFe_{1-x}Ga_xO_2$ [23], which have electromagnon resonances in the long-wavelength (pseudo)collinear magnetic phase. Significance of the mechanisms of the ME coupling for the adjacent type-II multiferroic phase has been suggested [22–24]. The latter material is exemplified by $Ba_2CoGe_2O_7$ in which the electric-field active excitation was observed even in the paramagnetic phase due to the crystal-field-like transition between Co^{2+} spin-orbital entangled multiplets [25–28].

For type-I multiferroics, however, the electromagnons tend to show up less conspicuously in the spectra as hexagonal $LuMnO_3$ [29] or often connect to complex magnetic structures, such as cycloidal magnetic order in $BiFeO_3$ [30,31] and non-collinear multisublattice ferrimagnetic order in $CaBaCo_4O_7$ [32]. Here we report one other type of electromagnon in a type-I multiferroic $Fe_2Mo_3O_8$ with a simple collinear magnetic order of magnetic moments of Fe^{2+} ions. We identify the mode characters of magnetic excitations including an electromagnon by the polarization selection rule as well as by the comparison with the ferrimagnetic phase induced by chemical doping or by the magnetic field. We propose a model of magnetic excitations, which consistently explains magnetic excitation in antiferromagnetic and ferrimagnetic phases. The modes are basically understandable as conventional antiferromagnetic resonances, but the ME coupling through the basal polar lattice turns a mode electric-field active, which extends the family of type-I multiferroics with the electromagnon.

$Fe_2Mo_3O_8$ forms a hexagonal lattice belonging to a polar space-group $P6_3mc$ [Fig. 1(a)]. There exist two types of magnetic site for the Fe^{2+} ion, A and B, characterized by the tetrahedral and octahedral coordinations of oxygen, respectively [33]. AO_4 and BO_6 polyhedra share their corners to form a honeycomb lattice on the ab plane. The two magnetic layers, which are related with a nonsymmorphic operation based on the c-glide plane with each other, are involved in the unit cell. Below the Néel point ($T_N = 60$ K) the system evolves into the collinear antiferromagnetic (AF) state [see the inset of Fig. 1(b)] [34]. Application of the magnetic -field (H_{dc}) along the c axis induces a collinear ferrimagnetic (FM) order

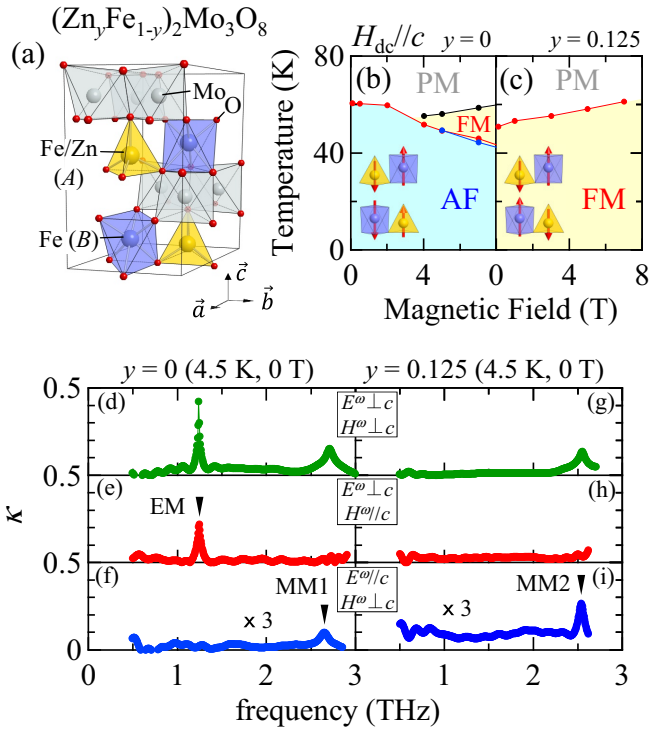

FIG. 1. (a) Crystal structure of $(Zn_yFe_{1-y})_2Mo_3O_8$. (b) and (c) Magnetic-field (H_{dc}) vs temperature phase diagrams under $H_{dc} \parallel c$ for $y = 0$ and $y = 0.125$, respectively, as reproduced from Ref. [36]. The magnetic structure of each phase is also shown. (d)–(i) Spectra of κ (imaginary part of the refractive index, i.e., extinction coefficient) for respective light polarizations at 4.5 K in a zero field (d)–(f) for $y = 0$ and (g)–(i) for $y = 0.125$.

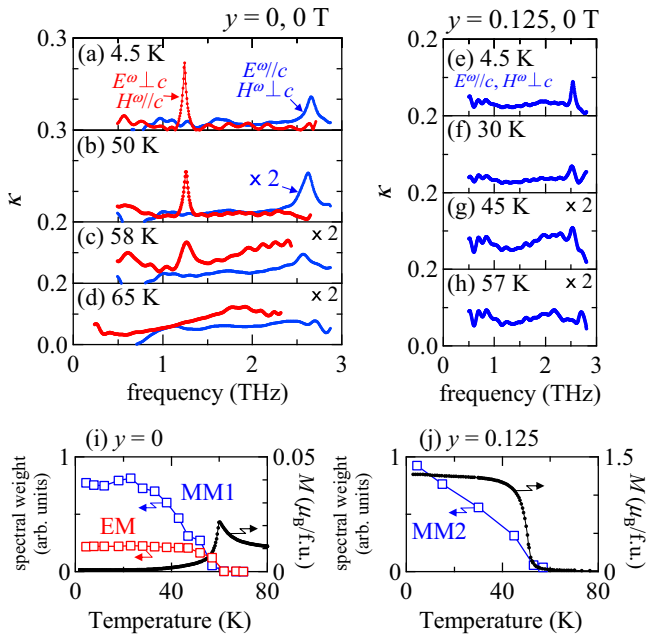

FIG. 2. (a)–(d) Temperature dependence of κ for $y = 0$ in a zero field. Red (blue) curves are for EM (MM1) measured with different light polarizations. (e)–(h) Corresponding spectra of $y = 0.125$ for MM2. Temperature dependence of spectral weight for (i) EM and MM1 and (j) MM2 in a zero field. Magnetization measured with $\mu_0 H_{dc} = 0.1$T also is shown for comparison.

[35,36] [the inset of Fig. 1(c)]. Alternatively, the FM state is stabilized also by substitution of more than 12.5% of Fe with Zn [34,36,37]. Coexistence of spontaneous polarization and magnetic order below the transition temperature allows strong ME coupling and large linear ME coefficients on both the *ab*-plane and the *c*-axis components, which promises the characteristic spin-wave excitation responding to the ac electric/magnetic fields of light.

Single crystals of $Fe_2Mo_3O_8$ and $(Zn_{0.125}Fe_{0.875})_2Mo_3O_8$ were grown by the chemical vapor transport reaction as described in Refs. [38,39] from the stoichiometric mixture of MoO_2,Fe,Fe_2O_3, and ZnO. Samples with *ab*-plane and *ac*-plane cuts, whose dimensions are typically $2 \times 2\,mm^2$, were prepared. The time-domain terahertz spectroscopy was employed to measure the refractive indices in a frequency range of 0.5–2.8 THz, and the details about the experimental setup and procedures are described in Ref. [40]. Laser pulses with 100-fs duration from a Ti: sapphire laser were split into two paths to generate and detect the wave form of terahertz pulses. A ZnTe (110) crystal and a dipole antenna were used for generation and detection of terahertz pulses, respectively. The H_{dc} was applied to the sample with a superconducting magnet in Voigt geometry, i.e., a light propagation vector k^ω perpendicular to H_{dc}.

Figures 1(d)–1(f) show the spectra of extinction coefficient κ (imaginary part of refractive index) for $Fe_2Mo_3O_8$ in a zero field at 4.5 K for three possible geometries. As shown in Fig. 1(d), two clear resonance peaks are observed around 1.2 and 2.7 THz for the light-polarized $E^\omega \perp c$ and $H^\omega \perp c$, denoted as EM and MM1, respectively. The characters of magnetic excitations can be deduced by the polarization selection rule derived from the results in Figs. 1(e) and 1(f); EM is concluded as electric dipole (E1) active, i.e., an electromagnon, because it can be excited by $E^\omega \perp c$ [(Fig. 1(e)] but not by $H^\omega \perp c$ [Fig. 1(f)], whereas MM1 is active for $H^\omega \perp c$ (not with $E^\omega \perp c$), indicating its magnetic dipole-(M1-) active nature. To check the correlation between the mode profile and the magnetic order, we also measured the spectra for the collinear ferrimagnetic phase in the doped sample ($y = 0.125$) [Figs. 1(g)–1(i)]. This composition shows the FM state even at a zero field [Fig. 1(c)]. A single resonance peak is observed around 2.6 THz (MM2) [Figs. 1(g) and 1(i)], whereas no discernible resonance structure is seen around 1.2 THz. Thus, the electromagnon resonance is absent [Fig. 1(h)] in the current energy window, whereas the MM2 is active for $H^\omega \perp c$ [Fig. 1(i)] similar to the MM1.

Figures 2(a)–2(h) show the spectra of κ for $y = 0$ and $y = 0.125$ at selected temperatures. With increasing temperature, the absorption of each mode gradually wanes and disappears above the transition temperature [Figs. 2(d) and 2(h)]. The temperature dependence of the spectral weights $[\propto -\frac{1}{d}\int \ln(t - t_0)d\omega]$ for the respective modes are shown in Figs. 2(i) and 2(j). Here, d is the thickness of the sample, t is the transmittance, and ω is the angular frequency of light. t_0 is assumed to be a background due to flat absorption. We define the spectral weights of EM, MM1, and MM2 by the integration among 1.1–1.4, 2.5–2.8, and 2.4–2.6 THz, respectively. The magnitude of these resonances starts to rise upon the magnetic ordering as shown in Figs. 2(i) and 2(j). This result indicates

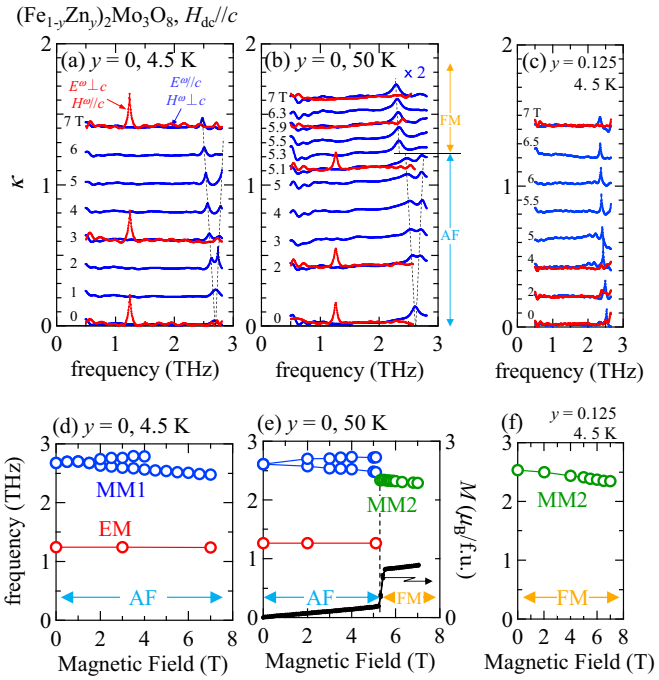

FIG. 3. (a)–(c) κ spectra under various field magnitudes. Data are shifted vertically for clarity. Red (blue) curves are for the polarization $E^{\omega} \perp c$ and $H^{\omega} \parallel c$ ($H^{\omega} \perp c$ and $E^{\omega} \parallel c$). Blue curves in (b) are magnified by 2. (d)–(f) Evolution of excitation frequency with $H_{\rm dc} \parallel c$: red, blue, and green circles are for EM, MM1, and MM2, respectively. In (e), magnetization along the c axis at 50 K is also shown for comparison.

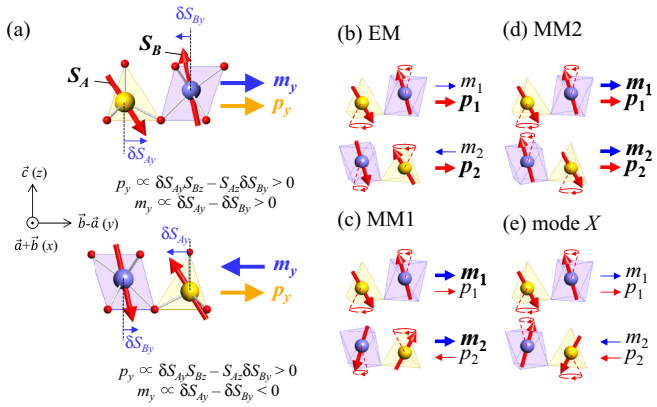

FIG. 4. (a) Schematic dynamical spin configurations with dynamical magnetization ($m_y \propto \delta S_{Ay} - \delta S_{By}$) and electric polarization ($p_y \propto \delta S_{Ay} S_{Bz} - S_{Az} \delta S_{By}$) oscillating on the c plane for upper and bottom layers in a unit cell. (b)–(e) Corresponding spin configurations for the respective magnetic excitation modes.

that the observed modes are collective excitations arising from the magnetic ordering and not from gap excitations related to the crystal field. Indeed, the latter excitation was observed in noncentrosymmetric $Ba_2CoGe_2O_7$ [26,27]. In this material, Co^{2+} forms a complex multiplet structure due to a strong spin-orbit interaction [25], resulting in the lowest Kramers doublet for effective spin $S_{\rm eff} = 1/2$ and another Kramers doublet locating at 4 meV above [26–28]. Transition between these two doublets acquires E1 activity observable even above the transition temperature unlike the case for $Fe_2Mo_3O_8$.

To clarify the mode characters in AF and FM states, the $H_{\rm dc}$ dependences of magnetic resonances are measured at selected temperatures as summarized in Fig. 3. Figure 3(a) shows κ spectra for the AF state [$y = 0$, see the phase diagram in Fig. 1(b)] at 4.5 K under $H_{\rm dc} \parallel c$ for two different light polarizations. Figure 3(d) shows field evolution of excitation frequency. EM shows little magnetic-field dependence, whereas the MM1 splits into two modes, implying the character of the conventional antiferromagnetic resonance. Although the EM may also be doubly degenerate, the possible frequency splitting appears to be too small to be detected for $\mu_0 H_{\rm dc}$ up to 7 T.

We also performed the comparative measurements for the FM state stabilized by the magnetic field at 50 K for $y = 0$ and by the chemical doping at 4.5 K for $y = 0.125$. The data sets are displayed in Figs. 3(b), 3(c), 3(e), and 3(f). At 50 K, $Fe_2Mo_3O_8$ shows the metamagnetic transition at $\mu_0 H_{\rm dc} \sim 5.2$ T as shown by the $M - H_{\rm dc}$ curve in Fig. 3(e). Upon the transition, the EM in $E^{\omega} \perp c$ geometry suddenly disappears, whereas the split lower-energy branch of the MM1 discontinuously turns into the mode (termed here MM2) with a slightly lower frequency [see the spectra for $\mu_0 H_{\rm dc} = 5.1$ and 5.3 T with $H^{\omega} \perp c$ in Figs. 3(b) and 3(e)]. On the other hand, the higher-energy branch appears to position at the outside of the present measurement range (>2.8 THz) where the excitation character has not been explored as yet. The excitation spectra of the MM2 mode in the FM phase also are exemplified by the FM phase induced by the chemical doping ($y = 0.125$) in which the monotonous softening of the MM2 is observed as the magnetic field is increased from 0 to 7 T [(Figs. 3(c) and 3(f)].

The emergence of the electromagnon mode in the AF phase indicates that the magnetic excitation possesses in-plane (on the plane perpendicular to the c axis) oscillation of electric polarization. The linear ME effect at the dc limit observed in the FM phase [36] can be related to the electrical activity of magnon excitation in the AF phase. Here, we consider two mechanisms for the linear ME effect as identified in Ref. [36], i.e., the inverse DM effect and the single-site anisotropy effect. Figure 4(a) shows the atomic configuration of the nearest-neighboring A and B sites in each upper and bottom honeycomb layer in a unit cell where the orthogonal xyz axes are defined with respect to the hexagonal unit vectors $\vec{a}$, $\vec{b}$, and $\vec{c}$. Although the conventional inverse DM model in Refs. [41,42] predicts P along the $c(z)$ axis for the adjacent spin on the A and B sites, the local site asymmetry in the present compound allows P in general directions, in accord with descriptions in Refs. [43,44]. In the present case, the symmetry with respect to the zy plane allows in-plane electric polarization p_y proportional to the dynamical x component of $\boldsymbol{S}_A \times \boldsymbol{S}_B$, i.e., $\delta S_{Ay} S_{Bz} - S_{Az} \delta S_{By}$. On the other hand, the single-site anisotropy effect [45,46] induces the in-plane polarization p_{iy} at each ith Fe site due to canting of a spin as $p_{iy} \propto S_{iz} \delta S_{iy}$.

Here we speculate possible modes of magnon excitations to explain the observed resonance including EM, MM1, and MM2. We ignore, to the first approximation, the interlayer magnetic interactions because the stacking honeycomb layers are intervened by a Mo layer. In each magnetic layer, spins at neighboring A and B sites prefer to oscillate in an

antiferromagnetic manner as shown schematically in Fig. 4(a). The neighboring spins cant with slightly different angles into the opposite direction as the result of single-ion anisotropy at each site. In this circumstance, electric polarization due to the inverse DM effect (p_y) is nonzero since the dynamical x component of $\boldsymbol{S}_A \times \boldsymbol{S}_B$ ($\delta S_{Ay} S_{Bz} - S_{Az} \delta S_{By}$) is nonzero, and the difference in the transverse component of the respective spins [δS_{Ay} and δS_{By} in Figs. 4(a)] induces a net magnetization m_y. Note that the mutual relation between m_y and p_y is opposite for the upper and bottom layers [Fig. 4(a)] in the unit cell since their relative positions are interchanged. Next, we take into account the interlayer coupling. In that case, doubly degenerate modes for the upper and bottom layers are coupled in an in-phase or an out-of-phase manner, resulting in the mode splitting. Figures 4(b) and 4(c) show in-phase and out-of-phase oscillations, respectively; m_y (m_1 and m_2) and p_y (p_1 and p_2) are shown for each layer. The oscillation pattern in Fig. 4(b) induces net p_y whereas m_y cancels; this explains why the EM can be excited by the in-plane electric field but not by the in-plane magnetic field of light. As for the out-of-phase oscillation [Fig. 4(c)], m_y remains finite, whereas p_y is canceled; this corresponds to MM1. Therefore, the configurations shown in Figs. 4(b) and 4(c) qualitatively explain the selection rule for the electromagnon and magnon modes observed in the AF phase. In Ref. [34], the interlayer coupling energies were estimated by the molecular-field theory, i.e., the antiferromagnetic interlayer coupling between A sublattices is stronger ($\sim$57 K) than that between A and B sublattices ($\sim$38 K). This is consistent with the lower excitation energy of EM than that of MM1; EM keeps the antiferromagnetic nature between interlayer A sites during the oscillation as shown in Fig. 4(b), whereas MM1 violates it [Fig. 4(c)]. Note that the in-plane electric polarizations due to the single-site anisotropy effect are uncanceled and canceled for the spin configurations in Figs. 4(b) and 4(c), respectively, giving the same conclusion on the dipole activities.

The above scheme is also applicable to the FM phase, which suggests both E1 and M1 active modes [Fig. 4(d)] as well as a silent mode [mode X as shown in Fig. 4(e)], although the experimentally observed MM2 appears to be M1 active but least E1 active. From the symmetry point of view, four magnetic excitation branches exist for a four-sublattice collinear magnetic system. Thus, we believe there is another higher-energy mode out of the range of this experiment which would show strong E1 and weak M1 activities, complementary to the nature of MM2. To confirm this, further spectroscopic studies for higher-frequency range and/or inelastic neutron-scattering experiments would be needed. In this Rapid Communication, we applied a simple model to capture elementary characters of the magnetic excitations in this system. Establishing the realistic spin Hamiltonian to theoretically reproduce the mode energy and electric/magnetic-fields susceptibility is also a significant future work.

In conclusion, we observe two distinct collective magnetic excitations driven by electric and magnetic fields of terahertz light, respectively, in the antiferromagnetic phase for polar magnet $Fe_2Mo_3O_8$. We also have revealed distinct properties of magnetic excitations for the antiferromagnetic and ferrimagnetic phases. The origin of the observed electromagnon is accounted for by the oscillation of electric polarization induced by precession of spins through the inverse Dzyaloshinskii-Moriya interaction and/or single-site anisotropy. Possible spin configurations for the excitations are suggested, which remain electric polarization uncanceled because of the out-of-phase interlayer coupling. The present observations show that a simple collinear magnetic order can host an electromagnon mode when spins order in a low-symmetric polar lattice to be a type-I multiferroic, which may be applicable on searches for other type-I multiferroics with electromagnons and with versatile optical magnetoelectric phenomena in the terahertz region as well as those in type-II multiferroics.

The authors thank Y. Okamura and L. Ye for enlightening discussions. This work was supported in part by JSPS Grant-In-Aid for Scientific Research(S) No. 24224009.

[1] J. F. Scott, J. Mater. Chem. **22**, 4567 (2012).
[2] F. Matsukura, Y. Tokura, and H. Ohno, Nat. Nanotechnol. **10**, 209 (2015).
[3] W. Eerenstein, N. D. Mathur, and J. F. Scott, Nature (London) **442**, 759 (2006).
[4] T. Kimura, T. Goto, H. Shintani, K. Ishizaka, T. Arima, and Y. Tokura, Nature (London) **426**, 55 (2003).
[5] J. Wang, J. B. Neaton, H. Zheng, V. Nagarajan, S. B. Ogale, B. Liu, D. Viehland, V. Vaithyanathan, D. G. Schlom, U. V. Waghmare, N. A. Spaldin, K. M. Rabe, M. Wuttig, and R. Ramesh, Science **299**, 1719 (2003).
[6] Y. Kitagawa, Y. Hiraoka, T. Honda, T. Ishikura, H. Nakamura, and T. Kimura, Nature Mater. **9**, 797 (2010).
[7] V. G. Bar'yakhtar and I. E. Chupis, Sov. Phys. Solid State **11**, 2628 (1970).
[8] A. Pimenov, A. A. Mukhin, V. Y. Ivanov, V. D. Travkin, A. M. Balbashov, and A. Loidl, Nat. Phys. **2**, 97 (2006).
[9] S. Dong, J.-M. Liu, S.-W. Cheong, and Z. Ren, Adv. Phys. **64**, 519 (2015).
[10] T. Kubacka, J. A. Johnson, M. C. Hoffmann, C. Vicario, S. de Jong, P. Beaud, S. Grubel, S.-W. Huang, L. Huber, L. Patthey, Y.-D. Chuang, J. J. Turner, G. L. Dakovski, W.-S. Lee, M. P. Minitti, W. Schlotter, R. G. Moore, C. P. Hauri, S. M. Koohpayeh, V. Scagnoli, G. Ingold, S. L. Johnson, and U. Staub, Science **343**, 1333 (2014).
[11] Y. Takahashi, R. Shimano, Y. Kaneko, H. Murakawa, and Y. Tokura, Nat. Phys. **8**, 121 (2012).
[12] D. Khomskii, Physics **2**, 20 (2009).
[13] B. B. van Aken, T. T. M. Palstra, A. Filippetti, and N. A. Spaldin, Nature Mater. **3**, 164 (2004).
[14] T. Goto, T. Kimura, G. Lawes, A. P. Ramirez, and Y. Tokura, Phys. Rev. Lett. **92**, 257201 (2004).
[15] G. Lawes, A. B. Harris, T. Kimura, N. Rogado, R. J. Cava, A. Aharony, O. Entin-Wohlman, T. Yildrim, M. Kenzelmann, C. Broholm, and A. P. Ramirez, Phys. Rev. Lett. **95**, 087205 (2005).
[16] K. Taniguchi, N. Abe, T. Takenobu, Y. Iwasa, and T. Arima, Phys. Rev. Lett. **97**, 097203 (2006).

[17] N. Kida, D. Okuyama, S. Ishiwata, Y. Taguchi, R. Shimano, K. Iwasa, T. Arima, and Y. Tokura, Phys. Rev. B **80**, 220406 (2009).
[18] A. B. Sushkov, R. V. Aguilar, S. Park, S.-W. Cheong, and H. D. Drew, Phys. Rev. Lett. **98**, 027202 (2007).
[19] A. B. Sushkov, M. Mostovoy, R. Valdés Aguilar, S.-W. Cheong, and H. D. Drew, J. Phys.: Condens. Matter **20**, 434210 (2008).
[20] S. P. P. Jones, S. M. Gaw, K. I. Doig, D. Prabhakaran, E. M. Hétroy Wheeler, A. T. Boothroyd, and J. Lloyd-Hughes, Nat. Commun. **5**, 3787 (2014).
[21] R. Valdes Aguilar, M. Mostovoy, A. B. Sushkov, C. L. Zhang, Y. J. Choi, S.-W. Cheong, and H. D. Drew, Phys. Rev. Lett. **102**, 047203 (2009).
[22] Y. Takahashi, S. Ishiwata, S. Miyahara, Y. Kaneko, N. Furukawa, Y. Taguchi, R. Shimano, and Y. Tokura, Phys. Rev. B **81**, 100413 (2010).
[23] S. Seki, N. Kida, S. Kumakura, R. Shimano, and Y. Tokura, Phys. Rev. Lett. **105**, 097207 (2010).
[24] M. Mochizuki, N. Furukawa, and N. Nagaosa, Phys. Rev. B **84**, 144409 (2011).
[25] A. Zheludev, T. Sato, T. Masuda, K. Uchinokura, G. Shirane, and B. Roessli, Phys. Rev. B **68**, 024428 (2003).
[26] I. Kezsmarki, N. Kida, H. Murakawa, S. Bordacs, Y. Onose, and Y. Tokura, Phys. Rev. Lett. **106**, 057403 (2011).
[27] S. Miyahara and N. Furukawa, J. Phys. Soc. Jpn. **80**, 073708 (2011).
[28] M. Soda, M. Matsumoto, M. Mansson, S. Ohira-Kawamura, K. Nakajima, R. Shiina, and T. Masuda, Phys. Rev. Lett. **112**, 127205 (2014).
[29] A. B. Souchkov, J. R. Simpson, M. Quijada, H. Ishibashi, N. Hur, J. S. Ahn, S.-W. Cheong, A. J. Millis, and H. D. Drew, Phys. Rev. Lett. **91**, 027203 (2003).
[30] M. Cazayous, Y. Gallais, A. Sacuto, R. de Sousa, D. Lebeugle, and D. Colson, Phys. Rev. Lett. **101**, 037601 (2008).
[31] I. Kezsmarki, U. Nagel, S. Bordacs, R. S. Fishman, J. H. Lee, Hee Taek Yi, S.-W. Cheong, and T. Room, Phys. Rev. Lett. **115**, 127203 (2015).
[32] S. Bordacs, V. Kocsis, Y. Tokunaga, U. Nagel, T. Room, Y. Takahashi, Y. Taguchi, and Y. Tokura, Phys. Rev. B **92**, 214441 (2015).
[33] W. H. McCarroll, L. Katz, and R. Ward, J. Am. Chem. Soc. **79**, 5410 (1957).
[34] D. Bertrand and H. Kerner-Czeskleba, J. Phys. (Paris) **36**, 379 (1975).
[35] Y. Wang, G. L. Pascut, B. Gao, T. A. Tyson, K. Haule, V. Kiryukhin, and S.-W. Cheong, Sci. Rep. **5**, 12268 (2015).
[36] T. Kurumaji, S. Ishiwata, and Y. Tokura, Phys. Rev. X **5**, 031034 (2015).
[37] S. Nakayama, R. Nakamura, M. Akaki, D. Akahoshi, and H. Kuwahara, J. Phys. Soc. Jpn. **80**, 104706 (2011).
[38] P. Strobel and Y. Le Page, J. Cryst. Growth **61**, 329 (1983).
[39] P. Strobel, Y. Le Page, and S. P. McAlister, J. Solid State Chem. **42**, 242 (1982).
[40] N. Kida, Y. Ikebe, Y. Takahashi, J. P. He, Y. Kaneko, Y. Yamasaki, R. Shimano, T. Arima, N. Nagaosa, and Y. Tokura, Phys. Rev. B **78**, 104414 (2008).
[41] H. Katsura, N. Nagaosa, and A. V. Balatsky, Phys. Rev. Lett. **95**, 057205 (2005).
[42] I. A. Sergienko and E. Dagotto, Phys. Rev. B **73**, 094434 (2006).
[43] T. Moriya, J. Appl. Phys. **39**, 1042 (1968).
[44] T. A. Kaplan and S. D. Mahanti, Phys. Rev. B **83**, 174432 (2011).
[45] G. T. Rado, Phys. Rev. Lett. **6**, 609 (1961).
[46] T. Arima, J. Phys. Soc. Jpn. **76**, 073702 (2007).